Discover Molecules

Research

Theoretical interpretation of electron delocalization potential of the substituent in o-hydroxynaphthalidene-p-substituted anilines for prospective molecular electronics applications

Supriya Priyambada Biswal[1] · Prabhudatta Hota[1,2] · Manas Ranjan Dash[3] · Pramila Kumari Misra[1]

Received: 19 March 2024 / Accepted: 1 July 2024
Published online: 27 August 2024

Abstract

The delocalization phenomenon plays a vital role in the electron transport properties of a molecule, which is essential for developing molecular-based electronics. The current work examined the delocalization potential of five theoretically designed low molecular weight anils, o-hyroxynaphthalidene-p-substitutedanilines(**NP-X**) with the substituent X(X = -CH_3, -NO_2, -OCH_3, and –Cl) being placed in phenyl ring at the p- position to its functional moiety, azomethine linkage and compared with the compound without substitution(X = H). The geometric optimization through DFT with B3LYP/6-311G (d, p) level basis set indicated the anils to be coplanar. Theoretical FTIR could discriminate the aromatic and aliphatic C-H vibrational frequencies and confirm the vectorial flow of the electrons when the o-OH group and p-NO_2 group were placed at the two extreme ends of anil, further supported by Natural Bond Orbital analysis. Atomic charge analysis indicated the significant effect on the charge of azomethine carbon atom. It followed the order: $OCH_3 < CH_3 < H < Cl < NO_2$ parallel with the σ_p values of the corresponding substituent. The molecular electrostatic potential mapping identified azomethine nitrogen as an electron-rich centre. The global and local reactivity parameters indicated the highest tendency of **NO_2** substituted compound to accept electrons among the other compounds. The HOMO–LUMO energy gap of the **NP-X** predicted from Natural Localized Molecular Orbital analysis was found to be **NP-H:** 4.02 eV, **NP-CH_3:** 3.94 eV, **NP-NO_2:** 3.69 eV**, NP-OCH_3:** 4.18 eV, **NP-Cl:** 4.10 eV. The overall studies corroborated the optimized delocalization in **NP-NO_2** with the lowest HUMO-LUMO gap, which would be better suited for developing molecular-based electronic devices than others. The importance of the electron delocalization phenomenon in searching for a molecular probe to develop molecular electronics device applications has been discussed.

This article is dedicated to Prof. B.K.Mishra, Retired Professor of School of Chemistry, Sambalpur University on his 70th Birthday.

Supplementary Information The online version contains supplementary material available at https://doi.org/10.1007/s44345-024-00002-8.

✉ Pramila Kumari Misra, pramilamisra@rediffmail.com | [1]Centre of Studies in Surface Science and Technology, School of Chemistry, Sambalpur University, Jyoti Vihar, Burla, Sambalpur, Odisha 768019, India. [2]Department of Chemistry, Boudh Model Degree College, Sarsara, Boudh, Odisha 762014, India. [3]Department of Chemistry, School of Physical Sciences, DIT University, Dehradun, Uttarakhand 248009, India.

Graphical Abstract

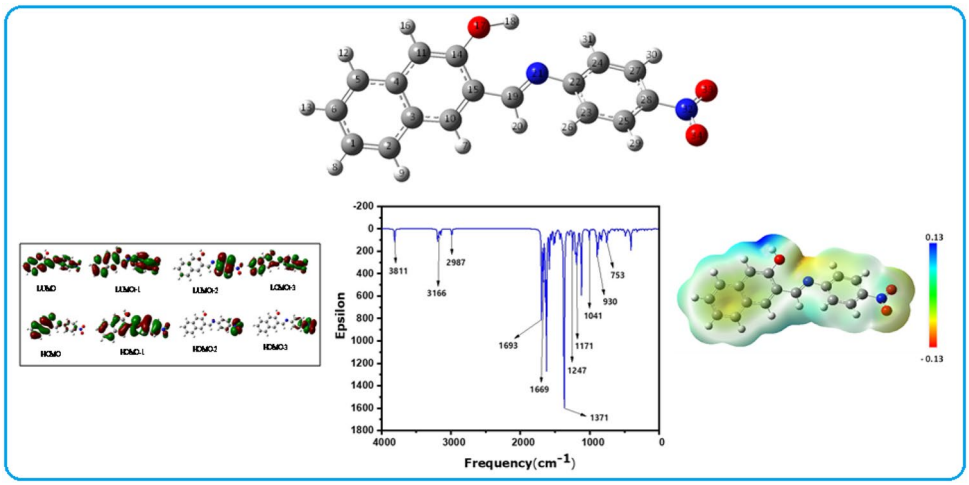

Keyword DFT studies · Global reactivity parameters · HOMO–LUMO energy profile · NBO & NLMO analyses · Molecular electrostatic potential

1 Introduction

Molecular electronics involving organic molecules is now an exhilarating field in interdisciplinary research spanning physics, chemistry, and material science due to the unifying features of organic molecules such as biodegradability, relatively high mechanical flexibility, less toxicity, easy synthetic procedure, and low cost in compared to the conventional electronics and requiring lower energy during the process of fabrication of the electrical components with desirable electrical properties [1]. Organic devices such as organic transistors, organic photovoltaic devices, liquid crystal displays, organic light emitting displays, biochemical sensors, and infrared imaging are a few examples where organic molecules have been successfully employed [2, 3]. The essential requirement for single molecule to realize these molecule-based devices is to exhibit electron-transport property. The delocalized electrons of the molecule spur the conductivity to the molecules [4], which in turn is modulated by the chemical structure of the molecule [5, 6]. Usually, the organic molecules with π-Conjugated molecular systems and heteroatoms like oxygen, sulphur and nitrogen show off electron transport property [7, 8]. The electron transport property of the molecules is reinforced further, depending on the nature of the substituent available in the molecule. The dichotomy exists in the system with the substituent that gives extra stability to the molecule by delocalizing the electrons over the whole molecular framework compared to the systems in which the charge is localized [9, 10]. The theoretical study of some designed benzo[1,2-*b*:4,5-*b'*]dithiophene-based molecules established that the optoelectronic properties were improved by substituting distinct acceptor moieties, including sulfur-, fluoro-, cyano-, and nitrogen-containing groups thiophene at both terminals of their unsubstituted analog [11]. Therefore, first-hand knowledge of the underlying mechanism of electron transport due to the substituent effect is indispensable for designing suitable organic components for electronic applications.

Anils are a particular class of Schiff bases in which the nitrogen atom of the azomethine functional group is directly linked to the phenyl ring [12, 13]. These molecules possess a donor-bridge-acceptor system, which is the essential criterion for a molecule to have electron-transport properties [14]. The distance, conjugation, and the nature of the donor/acceptor species and substituent affect the degree of interaction between the donor and the acceptor [15, 16]. Therefore, systematic investigation of the substituents at varying conditions for a set of donor and acceptor moieties in anils is vital for the accurate interpretation of a suitable device application [17, 18]. The azomthine is the suitable linking group which helps to lower the system's energy by delocalizing the electronic charges while transporting the electrons. The two phenyl rings(C-phenyl and N-phenyl) of their precursors from substituted/unsubstituted aromatic aldehyde with substituted/unsubstituted aromatic amine can donate electrons through the azomethine moiety

bridge depending on the nature of the substituent [19, 20]. Various properties of anils like hydrolytic [21–23], solvatochromism [24–27], keto-enol tautomerism [28], and acid–base behavior [29–31] have been explored depending on the nature and position of the substituents and accordingly their application perspectives have been ascertained [32]. However, the electron transport property is at its infant stage and has yet to be unveiled completely. Systematically investigating the anils with substituents of different electron affinities is highly desirable and challenging, especially in light of the recent drive to explore the application potentials of low molecular weight organic molecules in designing molecular electronic devices and optoelectronic applications [32–34].

These days, the development of computational procedures for estimating the potential of molecules for different applications is rising to avoid the hassle of synthesizing many molecules and minimize the wastage of chemicals, time, and human resources [35]. The primary dictum of the present work is to explore the electron transport behaviour of some selected anils (Fig. 1) theoretically by grafting their structure through suitable substituents in the aromatic ring of the amine part (N-phenyl ring), keeping the C-aromatic ring the same in all cases [12, 14]. In our recent paper [14], while analyzing the effect of chlorine substitution in the ortho position to the N-phenyl ring, significant electron transport behaviour of **Anil-1(**salicylidene-o-chloroaniline**)** and **Anil-2(**o-hyroxynaphthalidene-o-chloroaniline**)** was evident. The vibrational transitions relating to the C-H, C–OH, C-N, and C = N bonds were affected by substituting chlorine, which was found to be a mild donating substituent. Hota et al. [12] have analyzed the spectral characteristics of N-benzylideneanilines with $–OCH_3$ as the substituent reported a considerable effect of the substitution of the p–OCH_3 on comparing the theoretical and experimental vibrational and electronic frequencies with its unsubstituted analog. To acquire a wide-ranging depiction of the impact of substitution on the electron transport behaviour, the analysis of spectral properties of substitution of varying electron affinity seems obligatory. In particular, the resonance effect of an electron-withdrawing substituent in the para-position of the N-phenyl ring may decrease the electron density on the ring, which would, therefore, affect the electron delocalization in the reverse direction as against the electron-donating group. The vectorial flow of electrons over the entire molecular framework may also augment the electron transport tendency by keeping an electron-donating group in one end and an electron-withdrawing group in the other. Thus, the detailed structural analysis and structural stability of the anils with different p-substituents in the N-phenyl of anil may provide a comprehensive picture of the effect of substituents on the spectral and electron transport properties.

Biswal et al. [14] have theoretically revealed that the electron transport potential of **Anil-2** is superior to **Anil**-1 due to the facilitation of electron delocalization in the naphthyl unit in comparison to the phenyl ring in the former. Given the above facts, the present paper plans to conduct theoretical studies on the o-hyroxynaphthalidene-p-substitutedanilines (o-hydroxynaphthalideneaniline(**NP-H),** o-hydroxynaphthalidene-p-methylaniline(**NP-CH_3),** o-hydroxynaphthalidene-p-nitroaniline(**NP-NO_2),** o-hydroxynaphthalidene-p-methoxyaniline (**NP-OCH_3),** o-hydroxynaphthalidene-p-chloroaniline **(NP-Cl**) with the abbreviation as given in the bracket using Density functional theory for possible application as an optoelectronic material. The B3LYP/6-311G(d,p) level of theory was employed as the basis set. The optimized geometries, structural parameters, and vibrational transitions were analyzed. Further, global reactivity parameters and molecular electrostatic potentials, coplanarity of the molecules, and charge transfer interaction

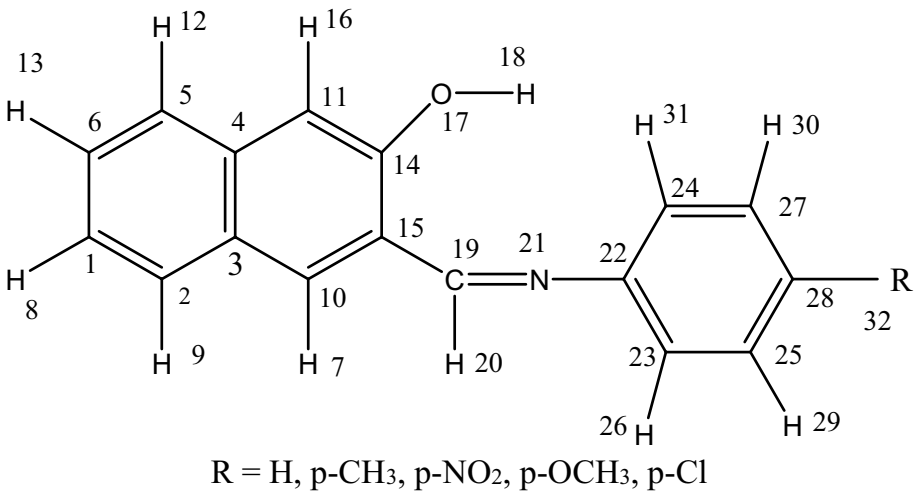

Fig. 1 Molecular structures of the focused anils, **NP-H: o**-hydroxynaphthalideneaniline, **NP-CH_3**: o-hydroxynaphthalidene-p-methylaniline, **NP-NO_2**: o-hydroxynaphthalidene-p-nitroaniline, **NP-OCH_3**: o-hydroxynaphthalidene-p-methoxyaniline, **NP-Cl**: o-hydroxynaphthalidene-p-chloroaniline

were also analyzed. The stability of the anils due to hyperconjugative interactions and charge delocalization was obtained from the natural bond orbital analysis.

2 Computational methods

The Gaussian program package (Gaussian 09 W) [36], which provides weightings of internal coordinates for vibrational assignments, was used for quantum mechanical calculations and optimization of the candidate molecules, orthohydroxynaphthalideneaniline, and its four substituted analogues, as presented in Fig. 1. The optimized structural parameters were obtained using DFT with Becke-3-Lee–Yang–Parr (B3LYP) basis sets of 6-311G (d, p) [37, 38]. The suitability of DFT/B3LYP using the 6-311G (d, p) basis set as the appropriate method for calculation was ascertained by comparing the bond length and bond angle values with the literature [14, 39–42]. DFT studies of N-benzylideneanilnes in our recently published article using this DFT functional and basis set pair were also found to match well with the experimental data [14].

3 Results and discussion

The substituent affects the delocalization of π-electrons because of physical phenomena like the mesomeric effect, inductive effect, and hyperconjugation. The substituent may be either electron-donating or withdrawing, depending on its inherent chemical entity and affinity towards the electrons [43]. The substituents like $–OCH_3$, CH_3, and NH_2 groups are electron-donating, whereas the substituents with π-bonds like $–NO_2$, $-COCH_3$, and CHO are electron-withdrawing. On the other hand, the substituents, like the Cl and OH groups, behave both electron-donating and electron-withdrawing due to chemical phenomena such as inductive and mesomeric effects depending on the chemical characteristics of the coupled moiety [39]. Reckoning with these facts, in the present investigation, five anils were selectively considered: **NP-H, NP-CH_3, NP-NO_2, NP-OCH_3,** and **NP-Cl**.

3.1 Molecular geometry optimization

Literature reports that molecular geometry has considerable influence on optoelectronic properties [44]. The five anils (Fig. 1) were subjected to quantum chemical calculations using the DFT (B3LYP) method with a 6-311G (d, p) basis set to obtain the corresponding optimized structures by using Gaussian 09 W. One representative optimized structure is given in Fig. 2. The rest of the optimized structures are given in Supplementary Material Figs. S1-S4. The corresponding calculated structural parameters are given in Supplementary Material Tables S1-S5.

The smooth electron delocalization, which in turn decides the flow of electrons over the whole molecular framework, depends primarily on the planarity of the molecule: the more planar the molecule is, the better the delocalization of the electron [45]. The planarity of the aromatic rings, i.e., C-naphthyl and N-phenyl ring in all anils, is ingenuously divulged as the bond angles of the sp^2 carbon atoms are either 120° or close to 120°[46]. Further, the coplanarity of the anils requires the C-naphthyl ring, the central molecular segment containing azomethine linkage, and the N-phenyl ring to lie in one plane, i.e., the dihedral angle in each case should be either zero or 180°[47]. In all anils, three different types

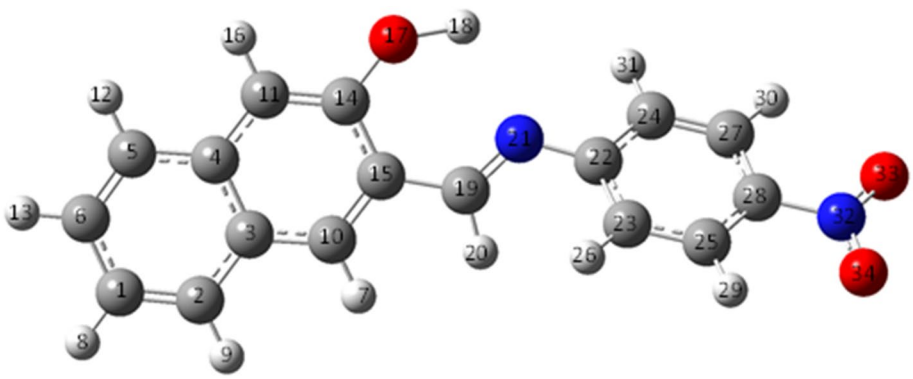

Fig. 2 Optimized structures of **NP-NO_2**

Table 1 Variation of dihedral angles of the focused molecules

Dihedral angle	**NP-H**	**NP-CH_3**	**NP-NO_2**	**NP-OCH_3**	**NP-Cl**
C14-C15-C19-N21	0.00	0.00	0.00	– 0.00	– 0.00
C10-C15-C19-N21	180	180	180	180	179.99
C15-C19-N21-C22	180	180	180	180	– 179.99
C19-N21-C22-C23	0.00	0.00	180	– 0.00	– 0.00
C19-N21-C22-C24	180	180	0.00	180	179.99

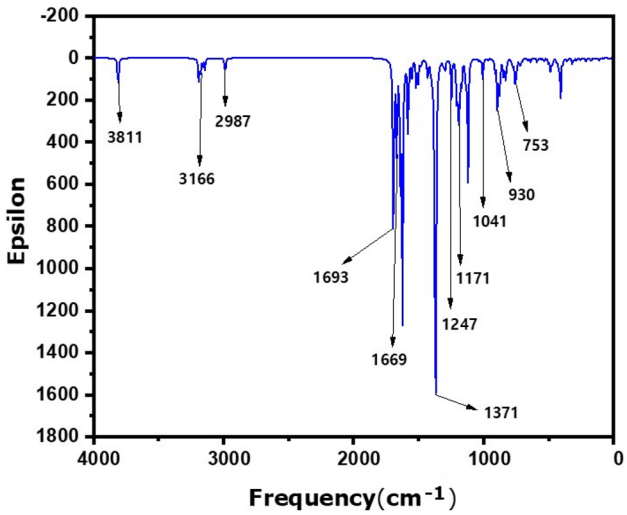

Fig. 3 Theoretical FTIR spectra of **NP-NO_2**

of dihedral angles are present: dihedral angle linked to C-naphthyl, i.e., ∠C14-C15-C19-N21, or ∠C10-C15-C19-N21, the central segment involving the azomethine group connecting C-naphthyl and N-phenyl rings, i.e., ∠C15-C19-N21-C22, and dihedral angle linked to N-phenyl ring, i.e., ∠C19-N21-C22-C23, or ∠C19-N21-C22-C24. These dihedral angles were abstracted from Supplementary Material Tables S1-S5 and are given in Table 1. On analyses, it is seen that the central dihedral angle is always 180° or nearly 180°, evidencing the planar nature of the segment. On the other hand, the dihedral angles involving C-naphthyl and N-phenyl rings, are either equal or close to 0° or 180°. These findings indicate that all the anils are coplanar. Hence, each anil possesses a suitable structural hierarchy for moving the π or lone pair of electrons over the molecular framework, as the case may be, to exhibit electron transport properties.

3.2 FTIR spectral analysis

The delocalization of electrons affects the strength of the bonds, and hence, the vibrational transition will be accordingly influenced. To delineate the extent of delocalization, the FTIR spectra were acquired theoretically in the ranges of 400 and 4000 cm^{-1} for the candidate anils, and one of the spectra is presented in Fig. 3. The rest are presented in Supplementary Figs. S5-S8. The specific bonds which were affected by delocalization were chosen for comparison. These values are provided in Table 2.

3.2.1 C-H vibration

The data in Table 2 demonstrates the stretching peaks appearing in the range 2979–3189 cm^{-1}, and bending peaks appearing in the range 1045–744 cm^{-1}. The aromatic and aliphatic C-H stretching vibrations were distinctly observed in the candidate anils, and the aliphatic C-H vibrations are always less than aromatic C-H vibrations because of the availability of π electron pools in the latter. The high electron density due to the π-electron pools at the carbon atoms possibly holds the hydrogen atom firmly, making the corresponding stretching vibrations greater than the aliphatic stretching vibrations. Further, it is seen that anil **NP-NO_2** experiences a distinctly different aliphatic C-H vibration stretching frequency compared to the rest of the four anils. In the latter cases, the frequencies

Table 2 Vibrational frequencies of different bonds of the candidate anils

Anils	C-H stretching frequency in cm^{-1}		C-H bending frequency in cm^{-1}
NP-H	2981–3159		1045–744
NP-CH_3	2980–3176		1041–757
NP-NO_2	2987–3166		1041–753
NP-OCH_3	2979–3189		1041–758
NP-Cl	2981–3177		1041–747
	O–H, C = N and C-N stretching frequency		
	O–H	C = N	C-N
NP-H	3811	1692	1241
NP-CH_3	3811	1691	1244
NP-NO_2	3811	1693	1247
NP-OCH_3	3810	1686	1242
NP-Cl	3811	1690	1243

of C-H vibrations are almost equal. Because the –OH group in the C-naphthyl ring pushes electrons towards the azomethine group, the flow is facilitated by the electron-withdrawing nature of nitro group, which is not possible in the rest of the anils. **NP-NO_2** exhibits a push–pull effect, whereas the rest of the anils exhibit a push-push effect during the electron delocalization except NP-H [27]. In NP-H, the lone pair of electrons on the oxygen atom in the –OH group is only pushed towards the azomethine group due to the higher electronegativity of the azomethine nitrogen atom. The nitro group substitution promotes the vectorial electron flow in **NP-NO_2**. The nitro group substitution also decreases the electron density at the aromatic carbon atoms, reducing the stretching frequency in nitro-substituted anil to a minimal value. On average, the stretching frequency follows the order: **NP-OCH_3** > **NP-CH_3** = **NP-Cl** > **NP-H** > **NP-NO_2** in line with the increasing order of electron-withdrawing nature of the substituted group, i.e., -OCH_3 > CH_3 = Cl > H > NO_2. Figure 4A represents the vectorial electron flow in **NP-NO_2**. This observation also suggests that chlorine acts as an electron-donating group, corroborating the observation obtained in our recent paper [14].

3.2.2 C–C, C = C, C-N, C = N, O–H Vibration

Generally, aryl chloride bands appear between 1100 cm^{-1} and 1035 cm^{-1} [48]. Similarly, aromatic methyl bands appear in the range 2962–2872 cm^{-1} [49], whereas the aromatic nitro bands appear in the range 1550–1490 cm^{-1} [49], and aromatic methoxy bands appear in the range 1050–1017 cm^{-1} [45]. In the present case, the C-CH_3 (**NP-CH_3**), C-NO_2 (**NP-NO_2**), C-OCH_3 (**NP-OCH_3**), and C–Cl (**NP-Cl**) stretching frequency occurs at 3099 cm^{-1}, 1371 cm^{-1}, 1064 cm^{-1}, and 1097 cm^{-1}, respectively corroborating the experimental values cited in the literature [38]. To investigate the effect of substitution on vibrational transition involving different functional groups present in the candidate anils, each of the vibrations is identified from the FTIR spectra and is presented in Table 2. C–C stretching frequency occurs in the range 1293–1668 cm^{-1} (**NP-H**), 1244–1663 cm^{-1} (**NP-CH_3**), 1247–1669 cm^{-1}(**NP- NO_2**), 1242-1667 cm^{-1} (**NP- OCH_3**), 1243–1668 cm^{-1} (**NP- Cl**), whereas C–C bending frequency occurs in the range 1190–930 cm^{-1} (**NP-H**), 1185–930 cm^{-1} (**NP-CH_3**), 1171–930 cm^{-1} (**NP- NO_2**), 1170–883 cm^{-1} (**NP- OCH_3**), 1190-881 cm^{-1} (**NP- Cl**).

The analysis of stretching frequencies of different vibrations, as demonstrated in Table 2, reveals that the –OH stretching frequency is not affected by the change in the nature of the substituent. Nitro-group substitution significantly affects the stretching frequency of both C = N and C-N vibration, and the values are highest among all the anils under consideration. This finding may be attributed to the increase in the electron density at the corresponding carbon atoms during electron delocalization. The electron-donating nature of the –OH group, coupled with further assistance by the electron-withdrawing nature of the nitro group increases the electron density at the azomethine carbon atom (Fig. 4A).

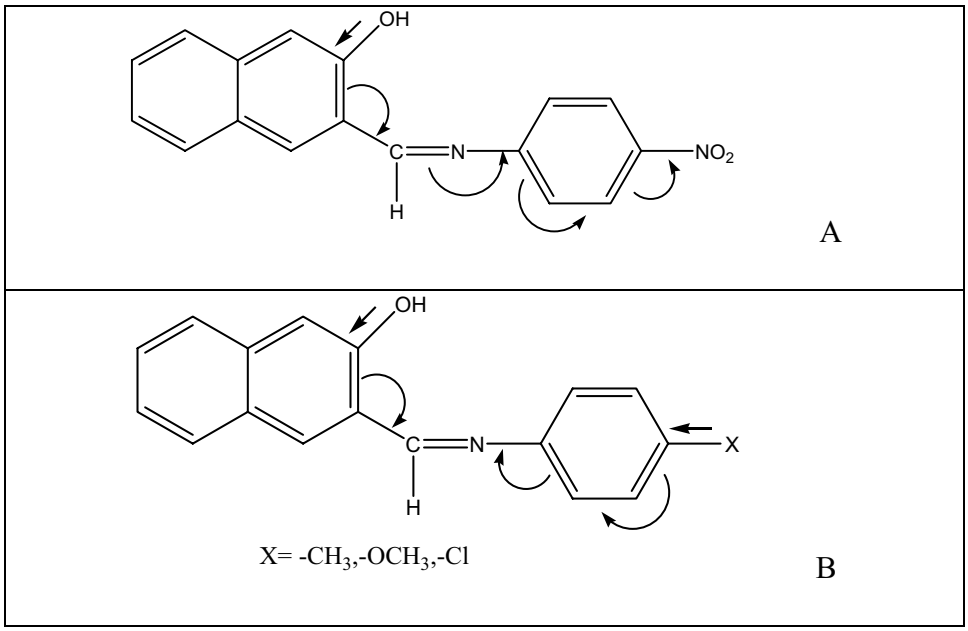

Fig. 4 Schematic representation of (**A**) the vectorial electron flow in **NP-NO$_2$**, and (**B**) Push-push effect in **NP-CH$_3$**, **NP-OCH$_3$**, **NP-Cl**

3.3 Natural bond orbital analysis

Natural bond orbital (NBO) analysis best illustrates the donor–acceptor interaction. The NBO analysis can determine the second-order perturbation energies of significant donor–acceptor interactions and depicts a precise knowledge of the electronic charge of each atom and the bond order between a pair of atoms [50, 51]. NBO analysis easily comprehends the total charge distribution on a molecule and the transfer of electrons from donor to acceptor moiety in a molecule [52]. From these data, an indirect evidence of the delocalization of electrons within a molecular system can be achieved. The second-order perturbation energies of significant donor–acceptor interactions of the candidate anils were calculated using Eq. 1 and are presented in Supplementary Tables S6-S10. The data were analyzed based on the general structure of anils presented in Fig. 1 in which C-naphthyl with an electron-donating substituent, –OH group is present in one terminus, and the N-phenyl group with a substituent of varying electron affinity is present in the other terminus.

$$E^{(2)} = \Delta E_{ij} = q_i F(i, j)^2 / \varepsilon i - \varepsilon j \quad (1)$$

From the FTIR spectral data, as discussed in the previous section, the vectorial flow of the electron delocalization in nitro-substituted anil is already evident (Fig. 4A). To corroborate this proposition further, the hyperconjugative interaction energy of the oxygen lone pair as donor orbital (π orbital) and C11-C14 as the acceptor orbital (π* orbital) in all anils were analyzed. It is seen that the interaction energy is at its maximum in the case of **NP-NO$_2$** (32.68 kcal mol^{-1}) with an electron-withdrawing substituent in the para position. In contrast, these values are lower in the anilines with electron-donating substituent (**NP-CH$_3$** = 28.58 kcal mol^{-1}, **NP-OCH$_3$** = 18.87 kcal mol^{-1}, **NP-Cl** = 18.85 kcal mol^{-1}). The **NP-H** without substituent has a moderate interaction energy value, i.e., 25.58 kcal mol^{-1}. Since the anils with electron-donating substituents exhibit a push-push effect (Fig. 4B), the smooth vectorial flow of electrons is obstructed, resulting in lower interaction energy. Although not promoted, this flow is not hindered in **NP-H;** hence**,** it attains a moderate interaction energy value.

Further, donor–acceptor interaction energy from carbon atoms connected to the substituent was analyzed to investigate the effect of the substituent in the opposite terminus (N-phenyl ring) on electron delocalization. The interaction energy between C25-C28/C23-C25: π orbital as donor orbital and C22-C23/C22-C24: π* orbital as the acceptor orbital is found to be lowest in **NP-NO$_2$** (16.62 kcal mol^{-1}). But these values are higher in anils with electron-donating substituents (**NP-CH$_3$** = 20.44 kcalmol^{-1}, **NP-OCH$_3$** = 19.80 kcalmol^{-1}, **NP-Cl** = 20.21 kcalmol^{-1}). The anil without substituent is found to have the intermediate value of energy (**NP-H** = 19.04 kcalmol^{-1}). This observation further supports that the electron flows in the direction shown in Fig. 4C for anils with electron-donating substituents. Since the nitro substituent in **NP-NO$_2$** drags the electron pool from the N-phenyl ring towards itself, this interaction energy lowers.

3.4 Atomic charges and molecular electrostatic potential map analysis

3.4.1 Atomic charges

The charge is distributed over the entire molecular skeleton during the delocalization phenomenon to lower the molecule's energy. Since the azomethine group is the functional unit of the anils under consideration through which the charge delocalization takes place, the impact of substituent on this moiety is a crucial point to consider. The Mulliken charges of each atom in the anils were abstracted from the optimized structures, presented in Fig. 5A and Supplementary Figs. S9-S12, and given in Table 3. Analysis of the magnitude and nature of charges reveals that the substituent significantly affects the charge of the azomethine carbon atoms. It follows the order: OCH_3(0.124) < CH_3(0.125) < H(O.126) < Cl(0.133) < NO_2(0.134), which is in line with the order of σ_p values: OCH_3(-0.268) < CH_3(-0.170) < H(0.00) < Cl (0.227) < NO_2(0.778) [53]. The rest of the atoms experience the usual effect due to the substitution.

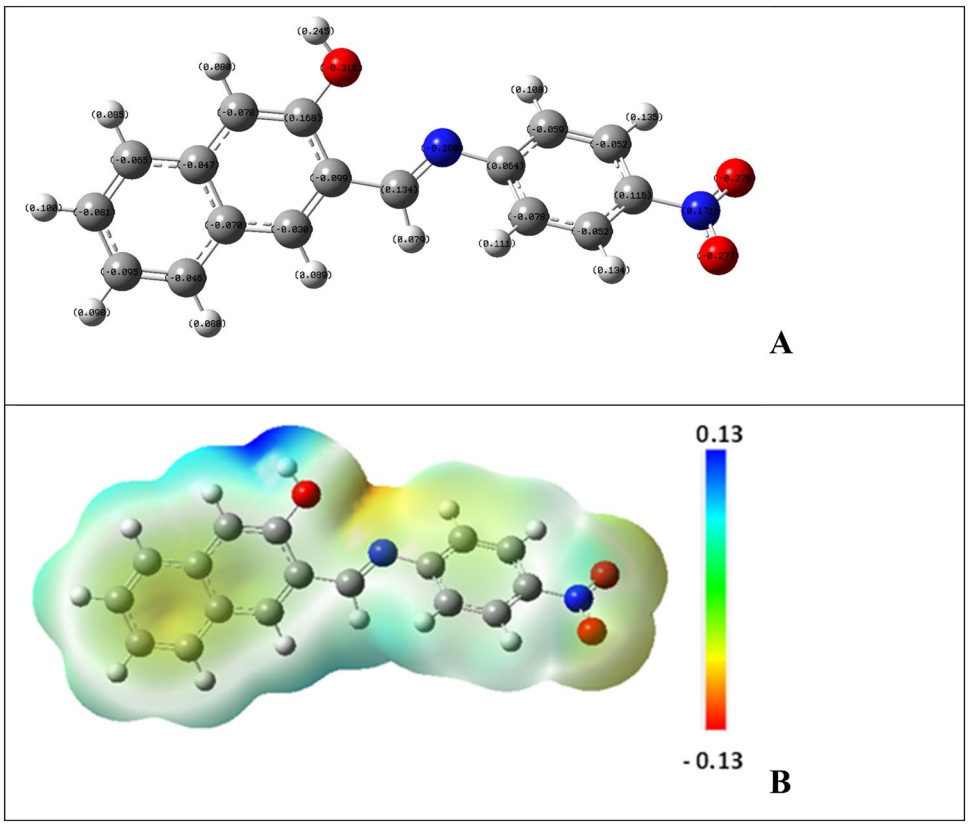

Fig. 5 Schematic representation of (**A**)Atomic charges and (**B**) Molecular electrostatic potential map of NP-NO_2, (Isovalue = 0.02)

Table 3 Mulliken charges on the atoms of candidate anils

Anils	Mulliken charges				Carbon atom linked to the substituent
	Oxygen atom	Nitrogen atom	Azomethine carbon	N-phenyl carbon linked to azomethine group	
NP-H	– 0.31	– 0.28	0.126	0.05	–
NP-CH_3	– 0.31	– 0.28	0.125	0.05	– 0.10
NP-NO_2	– 0.32	– 0.28	0.134	0.06	0.12
NP-OCH_3	– 0.31	– 0.29	0.124	0.04	0.17
NP-Cl	– 0.37	– 0.31	0.133	0.05	– 0.23

3.4.2 Molecular electrostatic potential map

A molecular electrostatic potential (MEP) signifies the electron density at the individual atom of a molecule. This map also relates to the polarity of the molecule [54]. The localization of electron density around particular regions makes it the most sensitive centre responsible for the exhibition of reactivity by a molecule [55]. Therefore, the site for electrophilic or nucleophilic attack in a chemical compound can be predicted by analyzing an MEP map visually. Identifying the electron-affluent atom and electron-deficient atoms, in particular, helps envision the directive flow of electrons during the delocalization. Hence, it can give insight into the electron transport property of a molecule. The molecule's size, shape, and electrostatic potential regions (positive, negative, and neutral) are analyzed in this energy map. The map represents the electrostatic potential at the molecule's surface with different colours. The potential increases according to the trend: red < orange < yellow < green < blue [56]. The MEP map of each anil was generated using the B3LYP/6-311G (d, p) level with a color range of + 0.13 to − 0.13. These plots are illustrated in Fig. 5B and Supplementary Figs. S13-S16. The red and blue areas on the surface refer to negative and positive potentials corresponding to the electron-rich and electron-deficient regions, respectively. The map analysis indicates that the blue region corresponds to the most positive hydrogen atom attached to the –OH group of the naphthyl ring. In contrast, the nitrogen atom occupies the most electronegative region as a dark red region. Thus, due to its high electron density, the nitrogen atom can be the site for electron/energy exchange during the fabrication of molecular-based electronic appliances [57]

3.5 Global and local reactivity descriptors

The global and local reactivity descriptors of a molecule best describe its structure–activity relationship [58]. Hence, these parameters can indirectly illuminate the electron transport behavior of a molecule. These descriptors depict the hardness (η), chemical potential (μ), electronegativity (χ), softness (S), and electrophilicity index (ω) of a molecule, which were calculated using Koopman's theorem for closed-shell molecules following Eqs. 2–6 given below considering the ground state optimized geometries in the gas phase of the candidate anils.

$$\eta = \frac{I - A}{2} \tag{2}$$

$$\mu = -\frac{(I + A)}{2} \tag{3}$$

$$\chi = \frac{(I + A)}{2} \tag{4}$$

$$S = \frac{1}{\eta} \tag{5}$$

Table 4 Molecular properties of candidate anils

Molecular properties	**NP-H**	**NP-CH_3**	**NP-NO_2**	**NP-OCH_3**	**NP-Cl**
E_{HOMO} (eV)	− 5.93	− 5.79	− 6.28	− 5.98	− 6.09
E_{LUMO} (eV)	− 1.90	− 1.85	− 2.58	− 1.79	− 1.98
$E_{LUMO-HOMO}$ (eV) Gap	4.02	3.94	3.69	4.19	4.10
Ionization Potential (I)	1.90	1.85	2.58	1.79	1.98
Electron affinity (A)	5.93	5.79	6.28	5.98	6.09
Chemical hardness (η)	− 2.01	− 1.97	− 1.85	− 2.09	− 2.05
Softness (S)	− 0.49	− 0.51	− 0.54	− 0.48	− 0.49
Chemical potential (μ)	− 3.92	− 3.82	− 4.43	− 3.89	− 4.04
Electronegativity (χ)	3.92	3.82	4.43	3.89	4.04
Electrophilicity index (ω)	− 3.81	− 3.70	− 5.31	− 3.61	− 3.97

$$\omega = \frac{\mu^2}{2\eta} \tag{6}$$

The estimated values of these parameters are provided in Table 4. The ionization potential (I.P.) for **NP-NO$_2$** is the highest among all, indicating the incredible difficulty in removing electrons from the molecule than the other anils, which is also supported by the highest electron affinity of **NP-NO$_2$** among the anils. The electronic chemical potential (μ) with the negative value in all studied anils indicates that these anils are more sensitive toward the change in the number of electrons. The value of global hardness (η) [59], which can be regarded as resistance to charge transfer, is − 1.85 eV to − 2.01 eV for the studied anils. Subsequently, the global softness (S), which measures the ease of charge transfer and is associated with high polarizability [60], is the lowest for **NP-NO$_2$** (− 0.54 eV). In contrast, it is highest for the **NP-OCH$_3$** (− 0.48 eV) among all the anils under consideration. The electrophilicity index, i.e., ω, measures the electrophilic power of a system. This parameter signifies the power of the electron-acceptor system to acquire the additional electronic charges from the environment [61]. The parameter is found to have a negative value in the range of − 5.31 eV to − 3.61 eV for the studied anils with the highest absolute magnitude value in the case of **NP-NO$_2$**. Therefore, assuming the studied system is an electron donor/acceptor system, the **NP-NO$_2$** has the highest tendency to accept electrons during the electron transfer reaction.

3.6 Natural localized molecular orbital analysis

The natural localized molecular orbital(NLMO) visualizes the interaction between the localized electrons and the vacant orbital, a vital charge delocalization entity. The plot is illustrated in Fig. 6. The NLMO calculations help in identifying the frontier molecular orbitals, i.e., highest occupied molecular orbital(HOMO) and lowest unoccupied molecular orbits(LUMO), that play a crucial role in optical, electrical, and chemical characteristics of a molecule [52]. Based on the NLMO calculations, the spread over of the electron densities on the frontier molecular orbitals(HOMO and LUMO) was identified(Supplementary Figs. S17-S20).

The HUMO-LUMO energy gap is decisive in determining molecular electrical transport properties because it measures electron conductivity [62]. The optoelectronic properties of a molecule can be optimized by tuning its HOMO–LUMO energy levels [63]. The energy gaps in between HOMO and LUMO in the studied anils are determined to be **NP-H:** 4.02 eV, **NP-CH$_3$:** 3.94 eV, **NP-NO$_2$:** 3.69 eV**, NP-OCH$_3$:** 4.19 eV, **NP-Cl:** 4.10 eV. The minimum energy gap value in NP-NO$_2$ predicts the optimized electron potential for developing molecular-based electronic devices [64, 65]. Mohammadi et al. [66] have also attributed a small energy gap in modified triphenyl diamine-based molecules due to the facilitation of

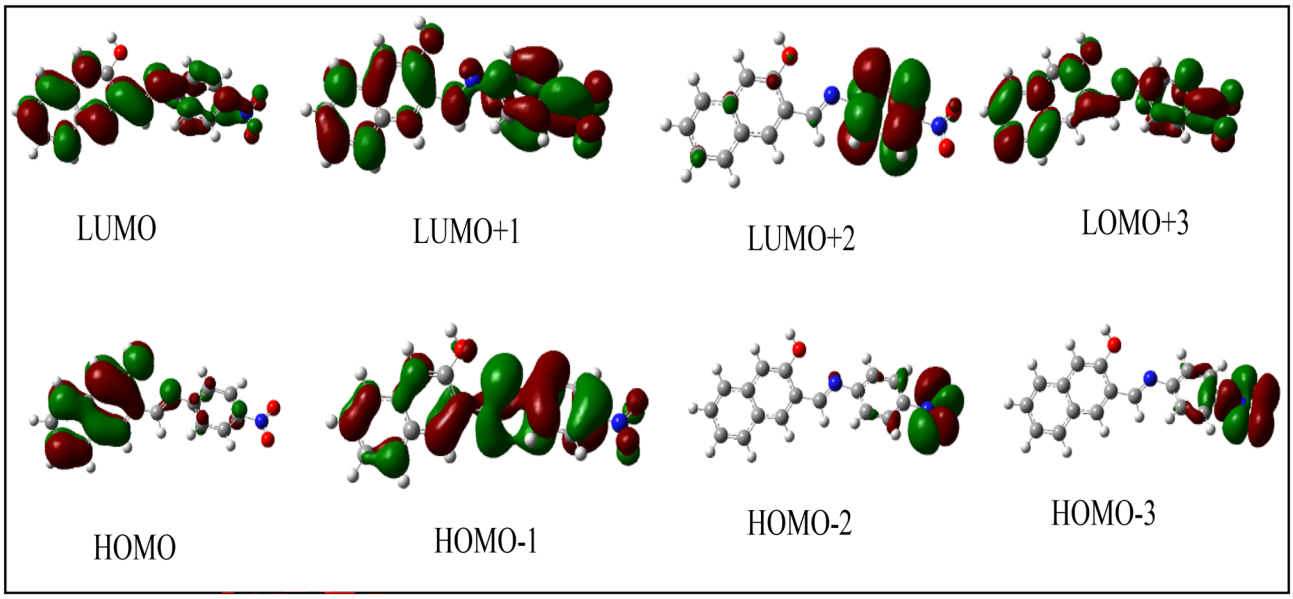

Fig. 6 NLMO of **NP-NO$_2$** (Isovalue = 0.02)

electron density flow from HOMO to LUMO and suggested their potential in optoelectronic capabilities of organic solar cells. The strong electron-withdrawing acceptor group usually results in the shifting of electron accumulation from HOMO to LUMO, yielding a significant decrease in the energy gap [44].

3.7 Electron delocalization-molecular electronics congenial relationship

Electron delocalization in a molecule creates free electron that moves freely within an orbital spanning several neighboring atoms. This property makes molecules conductive, forming the basis of molecular electronics. As a single molecule is the smallest plausible stable species, molecular electronics are essential for miniaturizing electrical circuits, a crucial objective for user-friendly products.

Organic molecules with heteroatoms like N, Si, O, S, and C = C double bonds or C≡C triple bonds are important for molecular electronics devices such as diodes, transistors, detectors, lasers, and microelectronics [67–69]. Anils (a special kind of Schiff bases with -C = N- directly linked to phenyl nucleus) with the centrally sandwiched azomethine linkage having aromatic rings at both ends enable electrons to move over the whole molecular framework vide the azomethine linkage. The movement of the lone pair of electrons and π-electrons of aromatic rings can be finely tuned when suitable substituents are positioned on either side. The conjugated system and the labile electron pair on the nitrogen atom facilitate electron delocalization, which can be triggered by applying an electrode potential. In turn, the charge carrier mobility of the molecule is enhanced which is the desired property of optoelectronic materials and hence this process opens up a world of intriguing molecular electronics. The resultant delocalized electrons can participate in electron transfer-initiated chemical reactions involving reduction and oxidations. Therefore, electron delocalization is a complementary phenomenon from the perspective of molecular electronics device applications. Literature reports many studies in which the conjugated Schiff bases and their complexes (with Cu and Zn) have been used in photonics and optoelectronic applications such as OLED [67, 70–72].

4 Conclusion

The research on the development of electronics devices involving organic molecules has received considerable attention these days due to several advantageous features of these molecules over conventional molecules. Understanding the structural parameters of the molecule by varying the substituent within it is an essential way of analyzing its suitability for desired applications. In the current paper, five anils, o-hydroxynaphthalidene-p-substituted anilines(**NP-X**) were examined theoretically using DFT-B3LYP functional theory with a 6-311G (d, p) level basis set. The anils with the substituent X as -CH_3, -NO_2, -OCH_3,-Cl group in the *para* position of the N-phenyl ring with respect to the azomethine linkage were compared with their unsubstituted analogue. The C-naphthyl ring contains a –OH group in the *ortho* position with respect to the azomethine linkage. The analysis of the optimized geometry relating to the dihedral angle of each anil envisages that the central dihedral angle involving the azomethine group connecting C-naphthyl and N-phenyl ring is always 180° or nearly 180°. In contrast, the dihedral angles linked to C-naphthyl and the dihedral angles linked N-phenyl rings, are either equal or close to 0° or 180°. These findings confirmed the coplanarity of all anils. FTIR reveals that the C-H stretching frequency follows the order **NP-OCH_3** > **NP-CH_3** = **NP-Cl** > **NP-H** > **NP-NO_2** in proportion to the increasing order of electron-withdrawing nature of the substituted group. However, the substituent change does not affect the OH stretching frequency. NBO analysis suggested the vectorial flow of electrons towards the substituent in **NP-NO_2**. The donor–acceptor interaction energy lowers in this molecule due to the dragging of electron pool from the N-phenyl ring by nitro substituent towards itself. Atomic charge analysis reveals the significant effect of substituent on the charge of azomethine carbon in the order: OCH_3(0.124) < CH_3(0.125) < H(O.126) < Cl(0.133) < NO_2(0.134), which is in line with the order of σ_p values. MEP analysis indicated high electron density on the nitrogen atom, which can be the site for exchanging electrons/energy. Global and local reactivity descriptors and NLMO analyses evidence that **NP-NO_2** has the highest tendency as an electron donor/acceptor system to accept electrons during the electron transfer reaction. The minimum HOMO–LUMO energy gap in **NP-NO_2** confirms its suitability for designing molecular-based electronic appliances. Overall, the theoretical studies reported in this work could be a helpful guide for achieving the long-term objective of economically fabricating single-molecular electronics devices. A synchronized analysis of electron delocalization in complex organic molecules using sophisticated DFT calculations, coupled with quantitative experimental determination of electrochemical properties, would further validate this proposition, either by us or by others in future.

Acknowledgements PKM thanks CSIR, New Delhi, for granting an Emeritus Scientist position at the School of Chemistry, Sambalpur University(Award No. 21(1141)/22/EMR-II), India. SPB thanks UGC, New Delhi, for financial support regarding the UGC-BSR junior and senior fellowship **(**F. No. 25-1/2014-15 (BSR)/7-166/2007/ (BSR).

Author contributions SPB and PKM have made a substantial contribution to the concept and design of study. SPB, PH, MRD, and PKM did all the acquisition, analysis and interpretation of data. SPB and PKM prepared the original draft of the manuscript.

Funding CSIR, New Delhi, (Award No. 21(1141)/22/EMR-II), & UGC, New Delhi,**(F. No. 25–1/2014–15 (BSR)/7–166/2007/ (BSR) for financial support.**

Data availability All data obtained through this work are tabulated in Supplementary Information.

Declarations

Competing interests No potential competing of interests was stated by the author(s).

References

1. Lee CW, Kim OY, Lee JY. Organic materials for organic electronic devices. J Ind Eng Chem. 2014;20:1198–208.
2. Kaushal JB, Raut P, Kumar S. Organic electronics in biosensing: a promising frontier for medical and environmental applications. Biosens. 2023;13:976.
3. Liu K, Ouyang B, Guo X, Guo Y, Liu Y. Advances in flexible organic field-effect transistors and their applications for flexible electronics. Npj Flex Electron. 2022;6:1.
4. Kitagawa Y, Tada H, Era I, Fujii T, Ikenaga K, Nakano M. Theoretical study on the difference in electron conductivity of a one-dimensional penta-nickel (II) complex between anti-ferromagnetic and ferromagnetic states-Possibility of molecular switch with open-shell molecules. Molecules. 2019;24:1956.
5. Silva CE, Pontes RB. Structural, electronic and transport properties of a single 1, 4-benzenediamine molecule attached to metal contacts of Au. Ag and Cu Comput Mater Sci. 2020;171:109212.
6. Pan S, Fu Q, Huang T, Zhao A, Wang B, Luo Y, Hou J. Design and control of electron transport properties of single molecules. Proc Natl Acad Sci. 2009;106:15259–63.
7. Wang C, Dong H, Jiang L, Hu W. Organic semiconductor crystals. Chem Soc Rev. 2018;47:422–500.
8. Yi W, Zhao S, Sun H, Kan Y, Shi J, Wan S, Wang H. Isomers of organic semiconductors based on dithienothiophenes: the effect of sulphur atoms positions on the intermolecular interactions and field-effect performances. J Mater Chem C. 2015;3:10856–61.
9. Sołtysiak P, Dziuk B, Zarychta B, Ejsmont K, Spaleniak G. The substituent effect of π-electron delocalization in N-methylamino-nitropyridine derivatives: crystal structure and DFT calculations. Struct Chem. 2020;31:1185–96.
10. Jain S, Danovich D, Radenkovic S, Shaik S. Dichotomy of delocalization/localization and charge-shift bonding in germanazene and its heavier group 14 analogues: a valence bond study. Chem Eur J. 2023;29: e202300992.
11. Mohammadi MD, Abbas F, Louis H, Amadu IO, Khalid M, Gber TE. Enhancing photovoltaic materials: DFT insights into structural modification of benzo [1, 2-b: 4, 5–b1] dithiophene unit (BDT)-based molecule. Comput Theor Chem. 2024;1231:114431.
12. Hota P, Biswal SP, Panigrahi S, Misra PK. Vibrational and electronic spectral analyses of substituted N-benzylideneanilines for possible application as material for a functional dyad: theoretical and experimental explorations. Mater Today Proc. 2019;9:680–8.
13. Panigrahi S, Misra PK. Kinetic study of some novel benzylideneanilines in homogeneous & heterogeneous environment. Int J Sci Res Innov. 2016;3:55–66.
14. Biswal SP, Hota P, Dash MR, Mahapatra A, Misra PK. Synthesis and characterization of tailor-made o-hydroxysubstituted anils through ^{1}H NMR, ^{13}C NMR, SC-XRD and DFT studies for possible optoelectronic applications. Mol Phys. 2023;121: e2225651.
15. Williams RM, Zwier JM, Verhoeven JW. Photoinduced intramolecular electron transfer in a bridged C60 (acceptor)-aniline (donor) system; photophysical properties of the first "active" fullerene diad. J Am Chem Soc. 1995;117:4093–9.

16. Kumar KS, Patnaik A. Thermodynamic, kinetic and electronic structure aspects of a charge-transfer active bichromophoric organofullerene. J Chem Sci. 2013;125:237–46.
17. Ilhan S, Baykara H, Seyitoglu MS, Levent A, Ozdemir SD, Undar A, Oztomsuk A, Cornejo MH. Preparation, spectral studies, theoretical, electrochemical and antibacterial investigation of a new Schiff base and its some metal complexes. J Mol Struct. 2014;1075:32–42.
18. Kilic A, Aydemir M, Durgun M, Meric N, Ocak YS, Keles A, Temel H. Fluorine/phenyl chelated boron complexes: synthesis, fluorescence properties and catalyst for transfer hydrogenation of aromatic ketones. J Fluor Chem. 2014;162:9–16.
19. Ledbetter JW Jr. Substituent effects on the tautomerism of Schiff bases. J Phys Chem. 1968;72:4111–5.
20. Furukawa S, Fujita M, Kanatomi Y, Minoura M, Hatanaka M, Morokuma K, Saito M. Double aromaticity arising from σ-and π-rings. Commun Chem. 2018;1:60.
21. Misra P, Mishra BK, Behera GB. Hydrolysis of Schiff bases, 1: kinetics and mechanism of spontaneous, acid, and base hydrolysis of N-(2/4-hydroxybenzylidene)-2-aminobenzothiazoles. Int J Chem Kinet. 1991;23:639–54.
22. Mishra P, Mishra BK, Behera GB. Hydrolysis of schiff bases 2: intramolecular catalysis of an ortho-hydroxy group in nonionic surfactant systems. Int J Chem Kinet. 1992;24:593–618.
23. Alcazar JJ, Geue N, Valladares V, Canete A, Perez EG, Garcia-Rio L, Santos JG, Aliaga ME. Supramolecular control of reactivity toward hydrolysis of 7-diethylaminocoumarin schiff bases by cucurbit [7] uril encapsulation. ACS Omega. 2021;6:10333–42.
24. Panigrahi S, Suna P, Misra PK. Effect of organized assemblies, part VIII: spectrophotometetric study on the effect of micellar media on the pK of some substituted N-benzylideneanilines. Coll Surf A Physicochem Eng Asp. 2012;415:349–57.
25. Suna P, Misra PK, Panigrahi S. Substituted benzylideneanilines: a family of solvatochromic probes. Spectrochim Acta Part A Mol Biomol Spectrosc. 2019;213:398–409.
26. Panigrahi S, Misra PK. The effect of solvent on electronic absorption bands of some benzylideneanilines. J Mol Liq. 2016;224:53–61.
27. Panigrahi S, Biswal SP, Misra PK. Disclosure of the solvatochromism and the reversal switch in some tailor-made electron push-push anils. J Mol Liq. 2021;329:115536.
28. Suna P, Hota P, Misra PK. Experimental and theoretical studies on the structure, electronic and vibrational spectra of o/p-hydroxybenzylidene-o/p-toluidines. Indian J Chem. 2016;55:1192–201.
29. Panigrahi S, Chakravorty M, Misra PK. Effect of organized assemblies: II. environmental effect on the pK of (o/p) hydroxybenzylidene-(4/6)-nitro-2-aminobenzothiazoles. J Coll Interface Sci. 2007;306:137–42.
30. Misra PK, Mishra BK, Behera GB. Determination of dissociation constants of salylidene-2-aminobenzothaizole and p-hydroxybenzylidene-2-aminobenzothiazole in different surfactant systems. Indian J Chem. 1988;27:889–92.
31. Mishra H, Misra P, Mishra AA. Variational approach to the gross-neveu model. Int J Mod Phys A. 1988;03:2331–8.
32. Yang Y, Wu Y, Bin Z, Zhang C, Tan G, You J. Discovery of organic optoelectronic materials powered by oxidative Ar–H/Ar–H coupling. J Am Chem Soc. 2024;146:1224–43.
33. Jeong M, Joung JF, Hwang J, Han M, Koh CW, Choi DH, Park S. Deep learning for development of organic optoelectronic devices: efficient prescreening of hosts and emitters in deep-blue fluorescent OLEDs. Npj Comput Mater. 2022;8:147.
34. Tas E, Onal IH, Yilmaz I, Kilic A, Durgun M. Synthesis, structural characterization, electrochemistry and spectroelectrochemistry of dinuclear copper (II) metal complexes stabilized by a tetradentate NOOO salicylaldimine ligands. J Mol Struct. 2009;927:69–77.
35. Rajendran P, Rathinasabapathy R, Chandra Kishore S, Bellucci S. Computational-simulation-based behavioral analysis of chemical compounds. J Compos Sci. 2023;7:196.
36. Frisch MJ, Trucks GW, Schlegel HB, Scuseria GE, Robb MA, Cheeseman JR, Fox DJ. Gaussian 09. Wallingford: Gaussian Inc.; 2009.
37. Ganaie JA, Sen N, Butcher RJ, Jasinski JP, Gupta SK. Synthesis, crystal structures, density functional theory (DFT) calculations and molecular orbital calculations of two new metal-free macrocyclic schiff bases derived from 2, 6-dibenzoyl-4-alkylphenol and diamines. J Chem Crystallogr. 2020;50:400–9.
38. Mohanty B, Das BR, Samal AK, Misra PK. Investigation of ethanol-phenol interactions used in steam reforming process: molecular level understanding through experimental and theoretical studies. Sustainable Chem Env. 2023;2:100006.
39. Pandit S, Dash MR. In pursuit of novel pyriporphyrin-a porphyrin ring expansion congener containing a built-in pyridine moiety by CH radical: a DFT investigation. Struct Chem. 2023;34:1457–68.
40. Dash MR, Mishra SS. Mechanistic and kinetics approach on methyl isocyanate (CH_3NCO) with OH and Cl. Mol Phys. 2022;120: e2124933.
41. Dash MR, Mishra SS. Theoretical kinetic studies of ethynyl radical with n-butane. J Phys Org Chem. 2021;34: e4249.
42. Dash MR, Srinivasulu G, Rajakumar B. Experimental and computational investigation on the gas phase reaction of p-cymene with Cl atoms. J Phys Chem A. 2015;119:559–70.
43. Michael BS, March J. March's advanced organic chemistry. 6th ed. Hoboken: Wiley-Interscience a John Wiley & Sons, inc. Publication; 2007.
44. Abbas F, Mohammadi MD, Louis H, Amodu IO, Charlie DE, Gber TE. Design of new bithieno thiophene (BTTI) central core-based small molecules as efficient hole transport materials for perovskite solar cells and donor materials for organic solar cells. Mater Sci Eng B. 2023;291:116392.
45. Szczepanik DW, Sola M. Electron delocalization in planar metallacycles: huckel or mobius aromatic? ChemistryOpen. 2019;8:219–27.
46. Georgiev A, Stoilova A, Dimov D, Yordanov D, Zhivkov I, Weiter M. Synthesis and photochromic properties of some N-phthalimideazo-azomethine dyes: a DFT quantum mechanical calculations on imine-enamine tautomerism and trans-cis photoisomerization. Spectrochim Acta Part A Mol Biomol Spectrosc. 2019;210:230–44.
47. Olalekan TE, Adejoro IA, Brecht BV, Watkins GM. Crystal structures, spectroscopic and theoretical study of novel schiff bases of 2-(methylthiomethyl) anilines. Spectrochim Acta Part A Mol Biomol Spectrosc. 2015;139:385–95.
48. Choudhary N, Bee S, Gupta A, Tandon P. Comparative vibrational spectroscopic studies, HOMO–LUMO and NBO analysis of N-(phenyl)-2, 2-dichloroacetamide, N-(2-chloro phenyl)-2, 2-dichloroacetamide and N-(4-chloro phenyl)-2, 2-dichloroacetamide based on density functional theory. Comput Theor Chem. 2013;1016:8–21.
49. Pavia DL, Lampman GM, Kriz GS, Vyvyan JR. Introduction to spectroscopy. 5th ed. Boston: Cengage Learning, Nelson Education Ltd; 2009.

50. AboAlhasan AA, El-Daly SA, Ebeid EZM, Sakr MA. Fluorescence quenching, DFT, NBO, and TD-DFT calculations on 1, 4-bis [2-benzothiazolyl vinyl] benzene (BVB) and meso-tetrakis (4-sulfonatophenyl) porphyrin (TPPS) in the presence of silver nanoparticles. Struct Chem. 2023;34:1265–77.
51. Rezvan VH, Aminivand Y. DFT computational study of optical properties for bis-Schiff bases of 8-aminoquinoline derivatives and furan-2,3-di-carbaldehyde. Struct Chem. 2024. https://doi.org/10.2139/ssrn.4183399.
52. Doust Mohammadi M, Abbas F, Arshad M, Shafiq F, Louis H, Unimuke TO, Rasaki ME. Increasing the photovoltaic power of the organic solar cells by structural modification of the R-P2F-based materials. J Mol Model. 2023;29:237.
53. Saleh BA, Essa AH, Al-Shawi SA, Jalbout AF. Correlation analysis of the substituent electronic effects on the Mulliken charge. Resonance and field effects of substituents at para-substituted styrenyl fullerene. J Mol Struct Theochem. 2009;909:107–10.
54. Gandhimathi S, Balakrishnan C, Venkataraman R, Neelakantan MA. Crystal structure, solvatochromism and estimation of ground and excited state dipole moments of an allyl arm containing schiff base: experimental and theoretical calculations. J Mol Liq. 2016;219:239–50.
55. Louis H, Eno EA, Timothy RA, Agwamba EC, Unimuke TO, Bukie PT, Offiong OE. Understanding the influence of alkyl-chains and heteroatom (C, S, O) doped electron-acceptor fullerene-free benzothiazole for application in organic solar cell: first principle perception. Opt Quantum Electron. 2022;54:681.
56. Soltani A, Ghari F, Khalaji AD, Lemeski ET, Fejfarova K, Dusek M, Shikhi M. Crystal structure, spectroscopic and theoretical studies on two schiff base compounds of 2, 6-dichlorobenzylidene-2, 4-dichloroaniline and 2,4-dichlorobenzylidene-2,4-dichloroaniline. Spectrochim Acta Part A Mol Biomol Spectrosc. 2015;139:271–8.
57. Hadi H, Gassoumi B, Nasr S, Safari R, Basha AA, Imran PM, Ghalla H, Caccamo MT, Ayachi S. Design, transport/molecular scale electronics, electric properties, and a conventional quantum study of a new potential molecular switch for nanoelectronic devices, ACS. Omega. 2024;9:1029–41.
58. Ramirez-Martinez C, Zarate-Hernandez LA, Camacho-Mendoza RL, Gonzalez-Montiel S, Meneses-Viveros A, Cruz-Borbolla J. The use of global and local reactivity descriptors of conceptual DFT to describe toxicity of benzoic acid derivatives. Comput Theor Chem. 2023;1226:114211.
59. Parr RG, Pearson RG. Absolute hardness: companion parameter to absolute electronegativity. J Am Chem Soc. 1983;105:7512–6.
60. Yang W, Parr RG. Hardness, softness, and the fukui function in the electronic theory of metals and catalysis. Proc Natl Acad Sci. 1985;82:6723–6.
61. Chattaraj PK, Sarkar U, Roy DR. Update 1 of: electrophilicity index. Chem Rev. 2007;107:2065–91.
62. Scharber MC, Sariciftci NS. Low band gap conjugated semiconducting polymers. Adv Mater Technol. 2021;6:2000857.
63. Abbas F, Mohammadi MD, Louis H, Agwamba EC. High-performance non-fullerene acceptor-analogues designed from dithienothiophen [3, 2-b]-pyrrolobenzothiadiazole (TPBT) donor materials. J Mol Model. 2023;29:31.
64. Agrawal AV, Kumar N, Kumar M. Strategy and future prospects to develop room-temperature-recoverable NO_2 gas sensor based on two-dimensional molybdenum disulfide. Nano-micro Lett. 2021;13:1–58.
65. Daoui S, Direkel S, Ibrahim MM, Tuzun B, Chelfi T, Al-Ghorbani M, Karrouchi K. Synthesis, spectroscopic characterization, antibacterial activity, and computational studies of novel pyridazinone derivatives. Molecules. 2023;28:678.
66. Mohammadi MD, Abbas F, Louis H, Ikenyirimba OJ, Mathias GE, Shafiq F. Advancing optoelectronic performance of organic solar cells: computational modeling of non-fullerene donor based on end-capped triphenyldiamine (TPDA) molecules. Comput Theor Chem. 2023;1226:114201.
67. Sıdır I, Sıdır YG, Khan N, Berber H. Optoelectronic and photonic properties of π-conjugated benzonitrile derivative bis-Schiff base by solution technique. Optik. 2021;241:166825.
68. Bin H, Yao J, Yang Y, Angunawela I, Sun C, Gao L, Li Y. High-efficiency all-small-molecule organic solar cells based on an organic molecule donor with alkylsilyl-thienyl conjugated side chains. Adv mater. 2018;30:1706361.
69. Petrus ML, Bein T, Dingemans TJ, Docampo P. A low cost azomethine-based hole transporting material for perovskite photovoltaics. J Mater Chem A. 2015;3:12159–62.
70. Amith Nayak PH, Bhojya Naik HS, Teja HB, Kirthan BR, Viswanath R. Synthesis and opto-electronic properties of green light emitting metal schiff base complexes. Mol Cryst Liq Cryst. 2021;722:67–75.
71. Wang L, Jiao S, Zhang W, Liu Y, Yu G. Synthesis, structure, optoelectronic properties of novel zinc Schiff-base complexes. Chin Sci Bull. 2013;58:2733–40.
72. Jeevadason AW, Murugavel KK, Neelakantan MA. Review on Schiff bases and their metal complexes as organic photovoltaic materials. Renew Sus Ener Rev. 2014;36:220–7.